

An optimal filter for the detection of galaxy clusters through weak lensing

Matteo Maturi^{1,2}, Massimo Meneghetti¹, Matthias Bartelmann¹, Klaus Dolag^{2,3}, Lauro Moscardini⁴

¹ ITA, Universität Heidelberg, Albert-Überle-Str. 2, 69120 Heidelberg, Germany

² Dipartimento di Astronomia, Università di Padova, Vicolo dell'Osservatorio 2, 35120 Padova, Italy

³ Max-Planck-Institut für Astrophysik, P.O. Box 1523, 85740 Garching, Germany

⁴ Dipartimento di Astronomia, Università di Bologna, Via Ranzani 1, 40127 Bologna, Italy

Astronomy & Astrophysics, submitted

Abstract. We construct a linear filter optimised for detecting dark-matter halos in weak-lensing data. The filter assumes a mean radial profile of the halo shear pattern and modifies that shape by the noise power spectrum. Aiming at separating dark-matter halos from spurious peaks caused by large-scale structure lensing, we model the noise as being composed of weak lensing by large-scale structures and Poisson noise from random galaxy positions and intrinsic ellipticities. Optimal filtering against the noise requires the optimal filter scale to be smaller than typical halo sizes. Although a perfect separation of halos from spurious large-scale structure peaks is strictly impossible, we use numerical simulations to demonstrate that our filter produces substantially more sensitive, reliable and stable results than the conventionally used aperture-mass statistic.

1. Introduction

Are there dark halos in the universe, i.e. dark-matter halos of substantial mass which for some reason fail to produce light? This question has recently attracted attention by the detection of significant and apparently massive peaks in weak-lensing surveys which are not seen to correspond to galaxy groups or clusters in the optical or X-ray bands (see e.g. Erben et al., 2000; Umetsu & Futamase, 2000; Miralles et al., 2002; Erben et al., 2003).

Dark-matter halos are embedded into large-scale structure. Measuring the inhomogeneities of projected mass distributions, lensing observations of halos are overlaid by the lensing signal of the large-scale structure in front of and behind the halos. Being approximately a Gaussian random field, lensing by large-scale structure adds peaks and troughs to the signal which can be mistaken for halos. It may thus be that part of the claimed dark-halo detections are in fact peaks in the random weak gravitational lensing signal of the large-scale structure.

Is there a way to separate the two types of lensing signal, and thus to improve the reliability of weak-lensing halo detections? The principal difficulty in doing so is the unsharp boundary between halos and the large-scale structure. Nonetheless, we shall describe below the construction of a linear matched filter which attempts to suppress the weak-lensing signal from large-scale structures and yet leaves the signal from sufficiently massive halos for detection.

Filtering in Fourier space is a flexible and powerful tool which has many applications for galaxy cluster lensing, like the lensing on the Cosmic Microwave Background radia-

tion, where there is a strong superimposition of different noise contributions (see e.g. Seljak & Zaldarriaga (2000) and Maturi et al. (2004)), and lensing on background sources. It could also be used for lensing on background galaxies.

Our strategy is as follows. The large-scale structure can be considered as composed of dark-matter halos of a broad and continuous mass range. Yet, there is a characteristic length scale at each cosmological epoch, the nonlinear scale, at which the variance of the dark-matter density contrast becomes unity. This length scale separates the small-scale regime where the dark-matter power spectrum is dominated by the contributions of presumably virialised halos from the large-scale regime on which the dark-matter density can be considered as a linear superposition of linearly evolved perturbation modes. In view of weak lensing, this suggests the operational definition of large-scale structure lensing which is contributed by the linearly evolved matter distribution beyond the non-linear scale, and halo lensing, which is contributed by non-linear, gravitationally bound, virialised structures.

We are aware that this operational definition may be questionable for many applications of weak gravitational lensing. For instance, it is well known that it is mainly the non-linear part of the dark-matter power spectrum which has now been measured with spectacular success in the weak-lensing surveys of many groups. Yet, we aim at a substantial more modest goal here. Being confronted with peak detections in weak-lensing data, we wish to know which of them can be attributed to halos, and which of them are likely caused by the large-scale structure.

In this attempt, we adopt the operational definition of the distinction between large-scale structure and halo lensing, construct a linear matched filter for halo lensing and model the lensing signal by intervening large-scale structures as a noise component influencing the shape of the matched filter. Matched filters for extracting sources of interest embedded into substantial background noise were previously proposed for many kind of observations, ranging from the analysis of Cosmic Microwave Background maps (Haehnelt & Tegmark, 1996; Tegmark & de Oliveira-Costa, 1998; Sanz et al., 2001; Herranz et al., 2002a,b; Schaefer et al., 2004) to weak lensing tomography (Hennawi & Spergel, 2004).

In Sect. 2, we briefly review those aspects of gravitational lensing which are needed for the rest of the paper. We describe the filter construction in Sect. 3 and contrast it with the more conventional aperture mass in Sect. 4. Simulations described in Sect. 5 are used in Sect. 6 to show that our suggested filter yields promising results. We summarise and conclude in Sect. 7.

2. Weak lensing quantities

We briefly review in this section those gravitational-lensing concepts which we shall use later. For a more detailed discussion, we refer the reader to the review by Bartelmann & Schneider (2001). We start with an isolated lens whose surface-mass density is $\Sigma(\theta)$ at the angular position θ on the sky. Its lensing potential is

$$\psi(\theta) = \frac{4G}{c^2} \frac{D_1 D_s}{D_{ls}} \int d^2\theta' \Sigma(\theta') \ln |\theta - \theta'|, \quad (1)$$

where $D_{1,s,ls}$ are the usual angular-diameter distances between the observer and the lens, the observer and the source, and the lens and the source, respectively. The reduced deflection angle experienced by a light ray crossing the lens plane at θ is the gradient of the potential,

$$\alpha(\theta) = \nabla\psi(\theta). \quad (2)$$

The image positions θ for a source located at β are given by the lens equation

$$\theta = \beta - \alpha(\theta). \quad (3)$$

For sources much smaller than typical scales on which the lens properties vary, the lens mapping can be linearised. The deformation of images with respect to the source is then given by the Jacobian matrix

$$A \equiv \frac{\partial\beta}{\partial\theta} = \left(\delta_{ij} - \frac{\partial^2\psi(\theta)}{\partial\theta_i\partial\theta_j} \right) = \begin{pmatrix} 1 - \kappa - \gamma_1 & -\gamma_2 \\ -\gamma_2 & 1 - \kappa + \gamma_1 \end{pmatrix}. \quad (4)$$

Here, κ is the convergence

$$\kappa(\theta) = \frac{\Sigma(\theta)}{\Sigma_{cr}} = \frac{1}{2} (\psi_{11} + \psi_{22}), \quad (5)$$

i.e. the surface-mass density scaled by its critical value

$$\Sigma_{cr} = \frac{c^2}{4\pi G} \frac{D_{ls}}{D_1 D_s}. \quad (6)$$

The distortion is described by the two components of the shear,

$$\gamma_1 = \frac{1}{2} (\psi_{11} - \psi_{22}), \quad \gamma_2 = \psi_{12}, \quad (7)$$

which are combined into the complex shear $\gamma \equiv \gamma_1 + i\gamma_2$. We further use the common abbreviation

$$\frac{\partial^2\psi(\theta)}{\partial\theta_i\partial\theta_j} \equiv \psi_{ij}. \quad (8)$$

Outside critical curves, image ellipticities are determined by the complex reduced shear

$$g(\theta) \equiv \frac{\gamma(\theta)}{1 - \kappa(\theta)}. \quad (9)$$

In the weak-lensing limit, $\kappa \ll 1$, and the reduced shear approximates the shear, $g \approx \gamma$, to first order.

Source and image shapes are quantified by the complex ellipticity

$$\epsilon = \frac{a - b}{a + b} e^{2i\theta}, \quad (10)$$

where a and b are the semi-major and semi-minor axes of an ellipse fitting the object's surface-brightness distribution. The position angle of the major axis of the ellipse is θ . The expectation value of the intrinsic source ellipticity ϵ_s is assumed to vanish.

A sufficiently small source with ellipticity ϵ_s is imaged to have an ellipticity

$$\epsilon = \frac{\epsilon_s + g}{1 + g^* \epsilon_s}, \quad (11)$$

where the asterisk denotes complex conjugation. This equation illustrates that the lensing distortion is determined by the reduced shear, which is the only lensing quantity directly accessible through measurements of galaxy ellipticities alone.

3. Filter construction

3.1. General description

We wish to construct a filter allowing the weak-lensing signal of halos to be extracted from weak-lensing observations of wide fields. We want the filter to suppress, as well as possible, the weak-lensing signal of the large-scale structure which can otherwise be mistaken as lensing by halos. As described in the introduction, we are well aware that this separation cannot fully succeed because of the unsharp boundary between lensing by large-scale structure and dark-matter halos. According to the operational definition of large-scale structure lensing given there, we shall model the weak lensing by linearly evolved structures as a noise component to be filtered out.

Consider the weak gravitational lensing signal of a dark-matter halo with amplitude A and angular shape $\tau(\theta)$. The measured signal $S(\theta)$ is contaminated by some noise $N(\theta)$,

$$S(\theta) = A\tau(\theta) + N(\theta), \quad (12)$$

whose components are to be specified below.

In our application, the observed signal is provided by the measured ellipticities of the background galaxies, which are weakly distorted by the foreground halo and the intervening large-scale structure. The expectation value of the image ellipticities at a given position on the sky is the reduced shear,

$$\langle \epsilon \rangle = g . \quad (13)$$

There are several noise contributions. First, the gravitational shear is being measured at the random positions of the background galaxies. This adds shot noise proportional to the number density of the galaxies. Second, these galaxies are intrinsically elliptical, thus the determination of a single galaxy ellipticity is a very noisy measurement of the shear only. This adds a noise component proportional to the variance of the intrinsic galaxy ellipticity. Finally, there is the noise component which we are primarily aiming at, which is caused by weak lensing of intervening large-scale structures. This third source of noise will be modelled by the linear dark-matter power spectrum, according to our operational separation between halo and large-scale structure lensing.

These noise components are assumed to be random with zero mean and isotropic such that their statistical properties are independent of the position on the sky. These assumptions are well justified, since in first approximation the background galaxies are randomly positioned and oriented, and weak lensing by the large-scale structures is well described by an isotropic Gaussian random field. The variances of the noise components are conveniently described in the Fourier domain, where their correlation functions are

$$\langle \hat{N}(\mathbf{k}')^* \hat{N}(\mathbf{k}) \rangle = (2\pi)^2 \delta(\mathbf{k}' - \mathbf{k}) P_N(k) ; \quad (14)$$

the hats above symbols denote the Fourier transforms.

We wish to construct a linear filter $\Psi(\boldsymbol{\theta})$ which, when convolved with the signal, will yield an estimate A_{est} for the amplitude A at the position $\boldsymbol{\theta}$,

$$A_{\text{est}}(\boldsymbol{\theta}) = \int S(\boldsymbol{\theta}') \Psi(\boldsymbol{\theta} - \boldsymbol{\theta}') d^2\theta' . \quad (15)$$

We further want the filter to satisfy two constraints. First, we require it to be unbiased, i.e. the average error,

$$b \equiv \langle A_{\text{est}} - A \rangle = A \left[\int \Psi(\boldsymbol{\theta}) \tau(\boldsymbol{\theta}) d^2\theta - 1 \right] \quad (16)$$

has to vanish. Second, the measurement *noise* σ , determined by the mean-squared deviation of the estimate from its true value,

$$\sigma^2 \equiv \langle (A_{\text{est}} - A)^2 \rangle = b^2 - \frac{1}{(2\pi)^2} \int |\hat{\Psi}(\mathbf{k})|^2 P_N(k) d^2k , \quad (17)$$

has to be minimal.

For finding a filter Ψ satisfying these two conditions, we combine them by means of a Lagrangian multiplier λ , carry out the variation of $L = \sigma^2 + \lambda b$ with respect to Ψ and thus find the function Ψ minimising L . The solution of this variational minimisation is given by

$$\hat{\Psi}(\mathbf{k}) = \frac{1}{(2\pi)^2} \left[\int \frac{|\hat{\tau}(\mathbf{k})|^2}{P_N(k)} d^2k \right]^{-1} \frac{\hat{\tau}(\mathbf{k})}{P_N(k)} . \quad (18)$$

This is the usual result showing that the optimal linear filter shape is determined by the shape τ of the signal, divided by the noise power spectrum. The filter is thus made most sensitive for those spatial frequencies where the signal $\hat{\tau}$ is large and the noise $P_N(k)$ is small.

3.2. Modelling the signal

Before we can apply this formalism to the observed data, we need to assume a model for the spatial distribution of the signal and a power spectrum describing the noise properties of the data. Concerning the signal, we assume that clusters are on average axially symmetric. Thus, $\tau(\boldsymbol{\theta}) = \tau(|\boldsymbol{\theta}|)$. Specifically, we use the density profile found in numerical simulations by Navarro et al. (1997) for modelling the average three-dimensional density profile of dark-matter halos,

$$\rho(r) = \frac{\rho_s}{(r/r_s)(1 + r/r_s)^2} , \quad (19)$$

where ρ_s and r_s are characteristic density and distance scales, respectively. These two parameters are not independent, but stochastically related to a single parameter, which can be chosen as the cluster mass.

The gravitational lensing properties of such a mass distribution have been widely explored (see e.g. Bartelmann, 1996; Meneghetti et al., 2003). Its lensing potential is given by

$$\psi(x) = 4\kappa_s h(x) , \quad (20)$$

with

$$h(x) = \frac{1}{2} \ln^2 \frac{x}{2} + \begin{cases} 2 \arctan^2 \sqrt{\frac{x-1}{x+1}} & (x > 1) \\ -2 \operatorname{arctanh}^2 \sqrt{\frac{1-x}{1+x}} & (x < 1) \\ 0 & (x = 1) \end{cases} , \quad (21)$$

where x is the projected distance from the lens centre in units of the distance scale, $x = r/r_s$. The reduced shear g is obtained from Eq. (20) using Eqs. (5) and (7). Its Fourier transform is defined as

$$\hat{\tau}(\mathbf{k}) \equiv \hat{g}(\mathbf{k}) = \int d^2x g(x) \exp(i\mathbf{x} \cdot \mathbf{k}) . \quad (22)$$

3.3. Noise power-spectrum

As discussed earlier, we take three sources of noise into account. These are the weak-lensing signal due to the large-scale structure, the shot noise from the finite number of randomly placed galaxies, and the noise due to the random intrinsic shape and orientation of the sources.

The weak gravitational lensing effect of the large-scale structures between the observer and the sources at a comoving distance w , observed in the direction $\boldsymbol{\theta}$ on the sky, gives rise to an effective convergence (see e.g. Bartelmann & Schneider, 2001)

$$\kappa_{\text{eff}}(\boldsymbol{\theta}, w) = \frac{3H_0^2 \Omega_m}{2c^2} \int_0^w dw' \frac{f_K(w-w') f_K(w')}{f_K(w)} \frac{\delta[f_K(w') \boldsymbol{\theta}, w']}{a(w')} \quad (23)$$

The factor out front contains the present-day matter-density parameter Ω_m and the Hubble constant H_0 . The comoving angular-diameter distance

$$f_K(w) = \begin{cases} K^{-1/2} \sin(K^{1/2}w) & K > 0 \\ w & K = 0 \\ (-K)^{-1/2} \sinh(K^{1/2}w) & K < 0 \end{cases} \quad (24)$$

is parametrised by the spatial curvature K . The density contrast $\delta = (\rho - \bar{\rho})/\bar{\rho}$ is taken at perpendicular distance $f_K(w')\theta$ and parallel distance w' , and $a(w')$ is the scale factor of the universe at distance w' .

When the sources are distributed in comoving distance, $\kappa_{\text{eff}}(\theta, w)$ needs to be averaged over the source-distance distribution $G(w)$,

$$\bar{\kappa}_{\text{eff}}(\theta) = \int_0^{w_H} dw G(w) \kappa_{\text{eff}}(\theta, w), \quad (25)$$

where the upper integration limit w_H is the comoving distance to the horizon.

The power spectrum of the effective convergence $P_\kappa(k)$ is related to the power spectrum of the three-dimensional density fluctuations $P_\delta(k)$ by Limber's equation,

$$P_\kappa(k) = \frac{9H_0^2 \Omega_m^2}{4c^2} \int_0^{w_H} dw \frac{\bar{W}^2(w)}{a^2(w)} P_\delta\left(\frac{k}{f_K(w)}, w\right), \quad (26)$$

in which the weight function $\bar{W}(w)$ is given by a line-of-sight integral over distance ratios,

$$\bar{W}(w) = \int_w^{w_H} dw' G(w') \frac{f_K(w' - w)}{f_K(w')}. \quad (27)$$

The cosmic-shear and effective-convergence power spectra are identical,

$$P_\gamma(k) = P_\kappa(k). \quad (28)$$

The noise contributions from random galaxy positions and ellipticities are both modelled as Poisson noise, which has a flat power spectrum. The shot-noise power spectrum from the galaxy positions is given by the number density n_g of suitable galaxies,

$$P_p(k) \propto \frac{1}{n_g}. \quad (29)$$

The noise component caused by the random intrinsic shape and orientation of the background galaxies has a power spectrum whose amplitude depends on the variance $\sigma_{\epsilon_s}^2$ of the intrinsic ellipticity distribution,

$$P_{\epsilon_s} \propto \sigma_{\epsilon_s}^2. \quad (30)$$

The two noise components are combined into one power spectrum which quantifies the noise of an ellipticity measurement,

$$P_\epsilon(k) = \frac{\sigma_{\epsilon_s}^2}{n_g}. \quad (31)$$

With the remaining noise components being independent, the total noise power spectrum is the sum of the contributions,

$$P_N(k) = P_\gamma(k) + P_\epsilon(k). \quad (32)$$

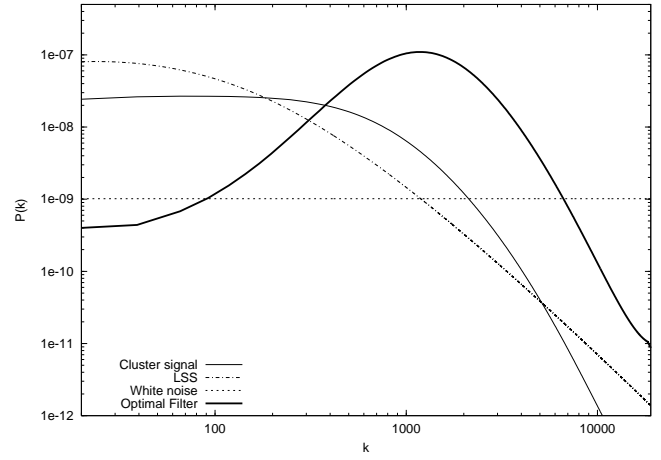


Fig. 1. Power spectra of the various components contributing to the definition of the optimal weak-lensing halo filter: effective convergence (dashed-dotted line), white noise composed of shot noise from the random galaxy positions and their intrinsic ellipticities (dotted line), and the model signal (solid line). The resulting filter is shown by the heavy solid line.

The contributions affecting the construction of the optimal filter are shown in Fig. 1. The solid line shows the power spectra of the signal, assuming an NFW lens model of $M = 5 \times 10^{14} h^{-1} M_\odot$ at redshift $z_l = 0.3$ and a source redshift $z_s = 2$. The effective shear power spectrum and the Poisson noise are given by the dash-dotted and the dotted lines, respectively, where the latter contains the contributions from the random galaxy positions and their random ellipticities. The bold solid line shows the filter resulting from Eq. (18). Unfortunately, but expectedly, the large-scale structure power is significant on those spatial frequencies where also most of the signal is located. This implies that it will be impossible to perfectly separate the true signal from the large-scale structure contaminations on the same scales. On the other hand, the lensing noise contributed by the large-scale structures on scales larger than the typical scale where the signal power spectrum becomes negligible will be effectively filtered away.

4. Aperture mass

For detecting halos through their weak-lensing signal, the aperture mass statistic (M_{ap} , Schneider, 1996) is frequently used. Due to its favourable statistical properties, it has turned into one of the prime tools for analysing cosmic-shear statistics. Its application to the detection of the weak-lensing patterns from dark-matter halos has been shown by several authors (see e.g Erben et al., 2000; Schirmer et al., 2004).

The aperture mass is a weighted integral of the local surface mass density,

$$M_{\text{ap}}(\theta) = \int d^2\theta' \kappa(\theta') U(\theta - \theta'), \quad (33)$$

where $U(\theta)$ is the weight function. If the aperture is chosen to be circular, U is axially symmetric, $U(\theta) = U(\theta)$. Since the

convergence is not directly measurable, Eq. 33 is conveniently rewritten in terms of the tangential shear γ_t as

$$M_{\text{ap}}(\theta) = \int d^2\theta' \gamma_t(\theta') Q(\theta - \theta'), \quad (34)$$

provided the filter U is *compensated*, i.e. satisfies

$$\int_0^\theta d\theta' \theta' U(\theta') = 0. \quad (35)$$

The function $Q(\theta)$ is related to $U(\theta)$ by

$$Q(\theta) \equiv \frac{2}{\theta^2} \int_0^\theta d\theta' \theta' U(\theta') - U(\theta). \quad (36)$$

The noise of the aperture mass is given by its variance

$$\sigma_{M_{\text{ap}}}^2 = \frac{\pi \sigma_{\epsilon_s}^2}{n_g} \int_0^\theta d\theta' \theta' Q^2(\theta'). \quad (37)$$

(Schneider, 1996).

The function U can be chosen such to maximise the signal-to-noise ratio $M_{\text{ap}}/\sigma_{M_{\text{ap}}}$. Schneider et al. (1998) show that this is the case if Q mimics the tangential shear profile of the lens. For example, Schirmer et al. (2004) use a function which approximates the expected shear profile of a NFW halo.

Thus, an assumption on the expected profile of the tangential shear needs to be made in the construction of both the optimal filter and the aperture mass. In this respect, the two functions U and τ should be chosen to look very similar. Two differences are important, however. First, the weight function U used in the definition of the aperture mass is compensated, while τ does not need to be. The reason is that the aperture mass was specifically defined such as to be proportional to the projected mass enclosed by the aperture. Our goal here is more modest as we only ask for significant halo detections, rather than for a determination of halo parameters apart from the overall shear amplitude. This allows us more freedom in the choice of τ compared to U . Second, the shape of the optimal filter differs from the profile function τ because it is modified by the shape of the total noise power spectrum. A comparison between the optimal filter and the function $Q(\theta)$ used by Schneider (1996) is shown in Fig. 2. The solid and the dot-dashed lines refer both to the optimal filter but for two different scale radii used for modelling the signal. We will show in the following sections how the two filters perform when applied to simulated data.

5. Simulated source catalogues

Numerical simulations are a unique tool for assessing the performance of the optimal filter, individually and in comparison to the aperture mass. In the following sections we describe the lens models and the numerical methods used for producing simulated catalogues of weakly distorted sources, subsequently analysed with our filter and the aperture-mass statistic.

5.1. Numerical models

The numerical model used here is a simulation of a super-cluster like region containing six halos with virial mass larger

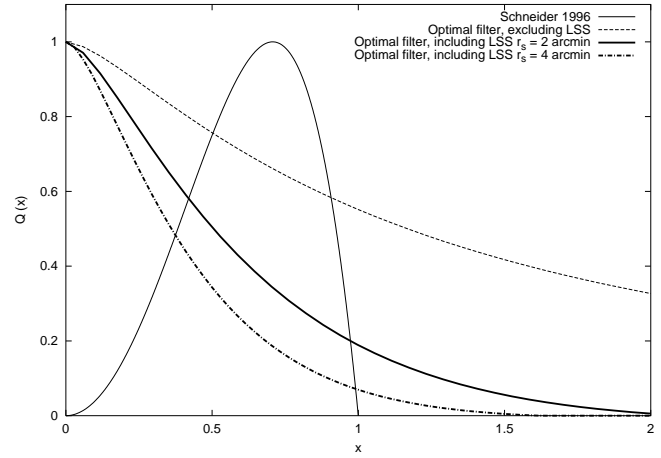


Fig. 2. Comparison between the filter profiles. Different lines refer to the conventional aperture mass (solid line), the optimal filter described in this paper but without the large-scale structure contribution to the noise power spectrum (dashed line), the full optimal filter for $r_s = 2'$ and $r_s = 4'$ (heavy solid heavy dot-dashed lines, respectively). The large-scale structure power spectrum modifies the filter shape according to the filter scale, by lowering its sensitivity on large scales where weak lensing by large-scale structure dominates.

than $5.6 \times 10^{13} h^{-1} M_\odot$. They are embedded in an over-dense region containing several less massive halos. The region is a section from an existing dark-matter only large-scale cosmological simulation, later re-simulated at higher resolution using the “Zoomed Initial Conditions” (ZIC) technique (Tormen et al., 1997). The parent simulation was an N -body run of a box of $479 h^{-1} \text{Mpc}$ side length containing 512^3 particles of mass $6.8 \times 10^{10} h^{-1} M_\odot$. The background cosmological model is spatially flat with $\Omega_m = 0.3$ and $\Omega_\Lambda = 0.7$ at the final epoch, identified with redshift zero (Yoshida et al., 2001; Jenkins et al., 2001).

From the output of this large cosmological simulation at redshift zero, we selected the super-cluster region for the following re-simulation. New initial conditions were constructed as follows. First, the particles contained in the selected region were traced back to their initial (Lagrangian) positions. These define a region in Lagrangian space. Then, the initial density field in that Lagrangian region was re-sampled by placing a higher number of particles than were originally present, adding additional small-scale power appropriately. Gas was introduced into the high-resolution region by splitting each parent particle into a gas and a dark-matter particle. The final mass resolution of these simulation was $m_{\text{DM}} = 1.13 \times 10^9 h^{-1} M_\odot$ and $m_{\text{gas}} = 1.7 \times 10^8 h^{-1} M_\odot$ for dark matter and gas within the high-resolution region, respectively. Thereby the simulation hosts a usable region of $25 h^{-1} \text{Mpc}$.

Finally, the region was evolved down to redshift $z = 0$ using the code GADGET-2, a new version of the parallel tree-SPH simulation code GADGET (Springel et al., 2001). The simulation was carried out including only non-radiative hydrodynamics. The comoving gravitational softening length was fixed to $\epsilon = 5.0 h^{-1} \text{kpc}$ (Plummer-equivalent).

For the present work, we use the output of the re-simulation at redshift $z = 0.297$. We separately analyse six sub-boxes, each of them centred on one of the six most massive halos. The comoving side-length of each sub-box was set to $\sim 14.45 h^{-1}$ Mpc, corresponding to 1° on the observer's sky.

5.2. Weak-lensing simulations

The particles in each sub-box sample a three-dimensional density field. Their positions are interpolated on a grid of 512^3 cells using the *Triangular Shaped Cloud* method (Hockney & Eastwood, 1988). Then, the three-dimensional density field is projected along its coordinate axes, thus producing three surface density maps, which we use as independent lens planes in the following lensing simulations.

The lensing simulations are performed by tracing a bundle of 2048×2048 light rays through a regular grid, covering the central quarter of the lens plane, corresponding to a field of view of 1° . The deflection angles $\alpha_{\text{sig}}(i, j)$ of each ray (i, j) are computed according to the method described in several earlier papers (see e.g. Meneghetti et al., 2000, 2001, 2004).

Weak gravitational lensing by large-scale structures between the observer and the sources is included as follows. From the power spectrum (26) of the effective convergence, we obtain the power spectrum of the effective lensing potential,

$$P_\psi(k) = \frac{4}{k^2} P_\kappa(k). \quad (38)$$

Since we only aim at measuring the efficiency of our filter for detecting a shear signal, the source redshift distribution is not important. Thus, all sources are assumed to be at the same redshift z_s , considering the two cases $z_s = 1$ or $z_s = 2$. The upper integration limit in Eq. (23) is then the comoving distance to the source plane, $w_s = w(z_s)$, and the distance distribution of the sources is a delta function,

$$G(w) = \delta(w - w_s). \quad (39)$$

We generate the effective lensing potential in Fourier space as a Gaussian random field. Using Eq. (2), we find the large-scale structure contributions to the deflection angles, $\alpha_{\text{LSS}}(i, j)$. The total deflection angle for each ray (i, j) is then

$$\alpha_{\text{tot}} = \alpha_{\text{sig}} + \alpha_{\text{LSS}}. \quad (40)$$

Reduced-shear maps for each field are straightforwardly derived from the deflection angle as explained in Sect. 2.

Background galaxies are randomly placed and oriented, and their ellipticities drawn from the distribution

$$p_s(|\epsilon_s|) = \frac{\exp\left[\left(1 - |\epsilon_s|^2\right)/\sigma_\epsilon^2\right]}{\pi\sigma_\epsilon^2 \left[\exp\left(1/\sigma_\epsilon^2\right) - 1\right]} \quad (41)$$

with $\sigma_\epsilon = 0.3$. We assume a background galaxy number density of $n_g = 25 \text{ arcmin}^{-2}$. Therefore, each field contains $\sim 90,000$ galaxies. ‘‘Observed’’ ellipticities are obtained from Eq. (11), and a catalogue containing the shapes and the positions of all sources in each field is compiled for the following analysis.

6. Results

6.1. Applying the filter

We now describe how we analyse the simulated catalogues. The integral in Eq. (15) is approximated by a sum over galaxy images. Since the ellipticity ϵ is an estimator for 2γ , we can write

$$A_{\text{est}}(\boldsymbol{\theta}) = \frac{1}{n_g} \sum_i \epsilon_{ti}(\boldsymbol{\theta}_i) \Psi(|\boldsymbol{\theta}_i - \boldsymbol{\theta}|), \quad (42)$$

where $\epsilon_{ti}(\boldsymbol{\theta}_i)$ denotes the tangential component of the i th galaxy's ellipticity relative to the line connecting $\boldsymbol{\theta}_i$ and $\boldsymbol{\theta}$. Thus, the filtering is performed in the real domain, which requires to Fourier back-transform the filter function from Eq. (18).

We measure A_{est} on a regular grid of 128×128 points covering the field. The noise estimate in A_{est} is obtained from

$$\sigma^2 [A_{\text{est}}(\boldsymbol{\theta})] = \frac{1}{2N^2} \sum_i |\epsilon_{ti}(\boldsymbol{\theta}_i)|^2 \Psi^2(|\boldsymbol{\theta}_i - \boldsymbol{\theta}|). \quad (43)$$

We produce maps of the signal-to-noise ratio (S/N) for all our fields. We then search for peaks with heights above a minimal S/N .

For comparison, similar signal-to-noise maps are produced using the aperture mass statistic. In this case, we also use Eqs. (42) and (43) for estimating the signal and the noise, but we substitute the filter function Ψ with the function Q discussed in Sect. 4.

6.2. Signal-to-noise maps

We show in this section how the filter performs on one projection of the field centred on the third most massive halo in the simulation box. The results for the fields centred on the other five halos are qualitatively and quantitatively very similar. The simulation we use represents a fairly complex case to study. Indeed, the field is crowded with ~ 15 subhalos of different masses and some filamentary structure connecting them.

Both the optimal filter and the aperture mass are designed for the optimal detection of halos of a given scale. For the optimal filter, this can be set to the scale radius of the NFW profile. However, this definition does not apply to the aperture mass. In fact, the size of the aperture is defined as the radius where the filter function Q has its first root. In order to compare the efficiency of the two filters for the detection of the same class of object, we have empirically adjusted the size of the aperture such that it resembles the scale of the signal profile used in the optimal filter.

We show in Fig. 3 the signal-to-noise contours for detections reaching above 5σ . The left and the right panels refer to the aperture mass and the optimal filter, respectively. From top to bottom, the filter scale is $1', 2', 4'$ for the optimal filter, corresponding to scales of $2.75', 5.5'$ and $11'$ for the aperture mass. In order to allow the reader to see which detections are real and which are spurious, we overlay the contours on surface-density maps from the numerical simulation. The halos which are identified by the halo finder are marked by circles with radii proportional to their virial radii.

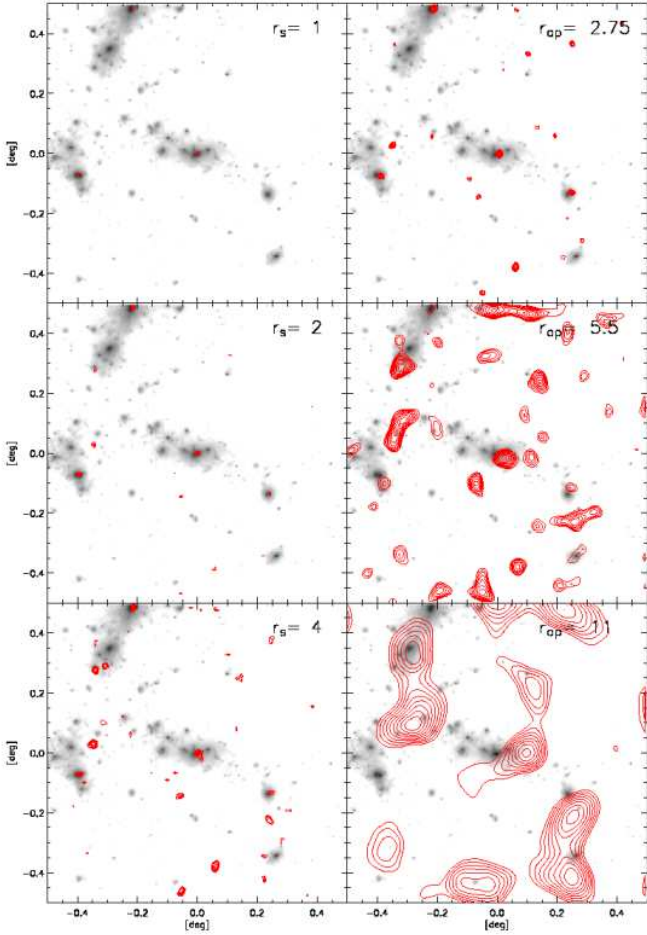


Fig. 3. Signal-to-noise contours above 5σ for different filter scales, assuming sources at redshift $z_s = 2$. Results obtained by applying the optimal filter and the aperture mass are shown in the left and right panels, respectively. From top to bottom, the scales are $1'$, $2'$ and $4'$ for the optimal filter, and $2.75'$, $5.5'$ and $11'$ for the aperture mass. The contours are overlaid in all panels on the surface-density map in the field centered on the third most massive halo in our simulation.

The optimal filter performs much better than the aperture mass in detecting the dark matter concentrations present in our simulated field. On all scales, the signal-to-noise ratios are larger for the optimal filter than for the aperture mass.

Spurious detections occur with both filters. A further inspection shows that these false matter concentrations are in fact connected to over-densities produced by the projection of the large-scale structures along the line-of-sight. As discussed in Sect. 3.3, these misidentifications cannot strictly be avoided, for the large-scale structure power spectrum is still large on the spatial scales where most of the signal resides. A possible method for discriminating between true halos and large-scale structure superpositions could be to group the sources in redshift bins. In fact, the large-scale structure pattern is expected to change for sources at different redshifts. This method is cur-

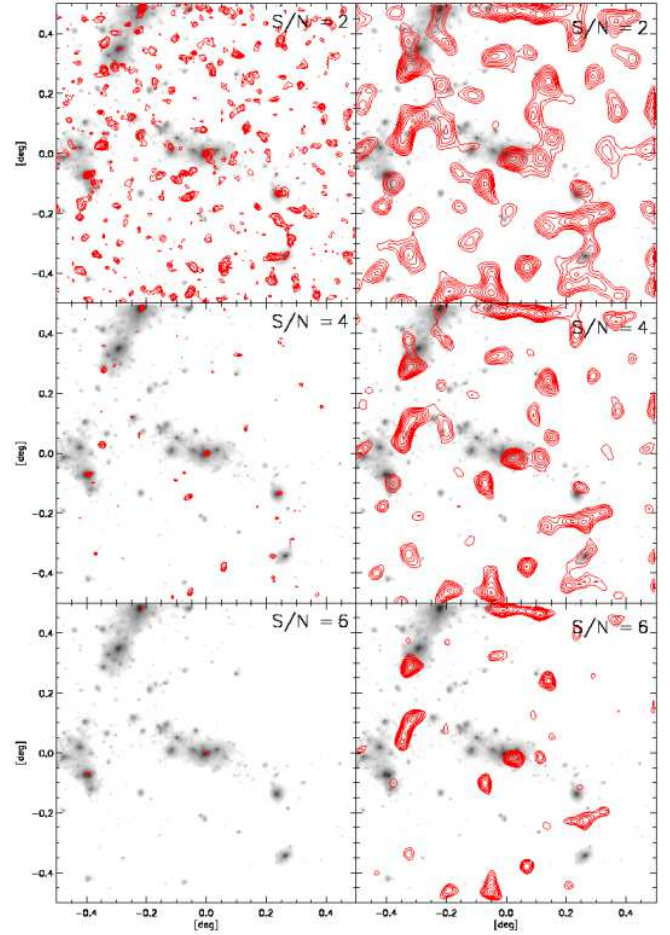


Fig. 4. Signal-to-noise contours for a fixed filter scale of $2'$ for the optimal filter (left panels) and of $5.5'$ for the aperture mass (right panels) for sources at redshift $z_s = 2$. From the top to the bottom panel, contours start at 2σ , 4σ and 6σ , respectively. In all panels, the contours are overlaid on the surface-density map in the field centered on the third most massive halo in our simulation.

rently being tested using numerical simulations (Meneghetti et al., 2005, in preparation).

It is remarkable that large-scale structure contaminations are much less important for the optimal filter compared to the aperture mass, especially when aiming at detecting clusters of large mass and low redshift, having large scale radii.

In Fig. 4, we show the detections above a minimal signal-to-noise ratio for a fixed filter scale of 2 arc minutes for our filter (right panels) and of 5.5 arc minutes for the aperture mass (left column). From the top to the bottom panels, the contours start at 2 , 4 and 6σ , respectively. Again, the efficiency of the optimal filter is remarkably higher than that of the aperture mass. No detections above 3σ are found with M_{ap} , while several true peaks are found using the optimal filter at more than 6σ .

Apparently the chance of a halo to be detected does not depend only on its mass or on the amplitude of the shear which it is able to produce. Indeed, the noise produced by the large-

scale structure can locally disturb the signal, such that even a relatively large halo can fall below detectability due to the local effective shear produced by the large-scale structure. As a simple test, we perform several weak-lensing simulations keeping the background galaxy population fixed and changing the large-scale structure in front of them, by using different realisations of the Gaussian random deflection-angle field. The results are shown in the sequence in Fig. 5 for sources redshift $z_s = 2$, and in Fig. 6 for $z_s = 1$. We use a filter scale of 2 arc minutes and plot the signal-to-noise contours above 4σ in all panels. In the right panels of images, the optimal filter is applied in order to remove the large-scale structure contamination. Clearly, some of the clumps which are detected for a given realization of the large-scale structure, are entirely missed when a different seed is used. For better illustrating the influence of the large-scale structures on the detection efficiency, we show in the left panels the same detections without including the large-scale structure noise in the construction of the optimal filter. Spurious halo detections are strongly reduced by using low-redshift sources because of the weaker large-scale structure contribution along the line-of-sight. This causes the signal-to-noise ratio to increase despite the clusters' being less efficient lenses for the lower-redshift sources. Compared to Fig. 5 the clusters' lensing efficiency is smaller because of the lower sources distance, but, for the same reason, there is a strong reduction in the large-scale structure contamination which leads to a gain in the signal-to-noise ratio.

7. Summary and discussion

We have developed a linear filter for detecting the weak-lensing signal of dark-matter halos. Given the expected shape τ of the halo signal, the filter is uniquely determined by the two requirements that it be unbiased and maximise the signal-to-noise ratio. The filter shape is modified by the noise power spectrum, into which we include the shot noise from the random positions of the galaxies used to measure the gravitational shear, the noise from their random intrinsic ellipticities, and the weak-lensing signal contributed by the large-scale structure. Since the total noise power spectrum is monotonically falling over the scale of the shape function τ , the inclusion of the noise narrows the filter considerably.

Our primary goals are to obtain a filter which separates halos from spurious peaks in the lensing effects of the projected large-scale structure, and whose results are stable against small changes in the filter scale. Our motivation is that applications of another statistic used for detecting dark-matter halos, the aperture mass M_{ap} , tend to detect large numbers of dark peaks, i.e. peaks in the lensing signal which are not found to correspond to detectable signal in the optical or X-ray wave bands. Moreover, these peak detections tend to be unstable against changes in the characteristic scale of M_{ap} , i.e. the significance of their detection may change wildly upon even small changes of scale.

It is clear that a clean separation of halos from large-scale structure is impossible because large-scale structure can be considered as being composed of dark-matter halos. We thus choose the operational definition that the halos we wish to de-

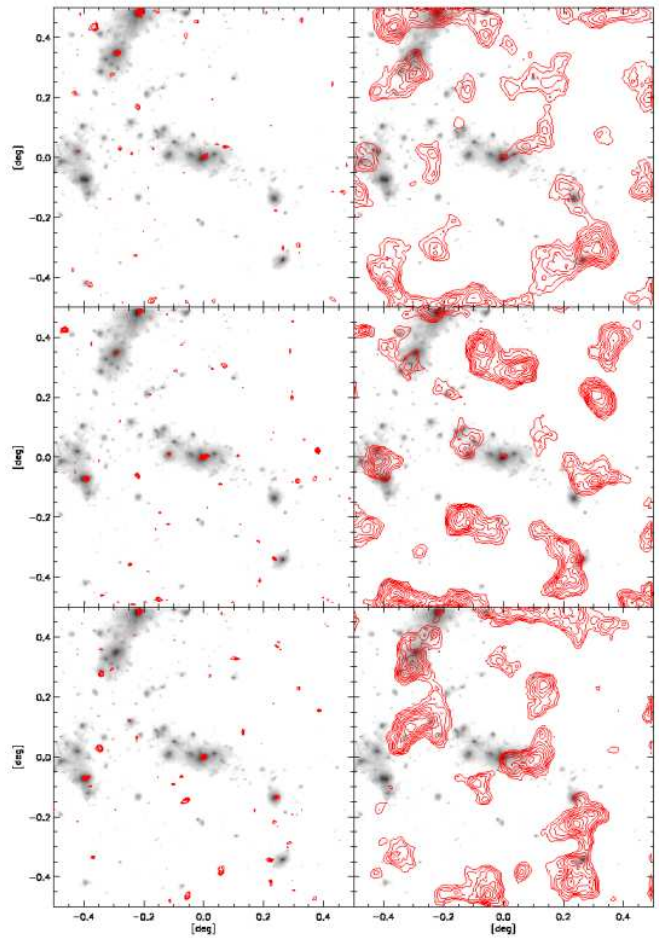


Fig. 5. Signal-to-noise contours above 4σ for different realizations of the large-scale structure. Results obtained by applying the optimal filter with and without filtering out the large-scale structure are shown in the left and in the right panels, respectively. The scale of the filter is $2'$ and the source redshift is $z_s = 2$.

tect are distinguished from large-scale structure as being objects on scales smaller than the non-linear scale. Consequently, we model the large-scale structure “noise” in the weak-lensing signal as being due to linearly evolved structures alone.

We perform numerical simulations for testing our new filter. The results, summarised in Figs. 3, 4 and 5, demonstrate that the filter meets all of our goals. Changes in the filter scale leave the signal much more stable than the aperture mass does, as Fig. 3 shows. Fig. 4 illustrates that the signal-to-noise ratio produced with our filter is typically substantially higher than that of the aperture mass, and Fig. 5 demonstrates that filtering halos against large-scale structure lensing is indeed very efficient. Compared to the aperture mass, the number of spurious peaks is also substantially reduced.

We thus propose this filter as an alternative statistic for detecting dark-matter halos. Of course, the aperture mass remains a very valuable statistic which has its significant strengths in analyses of lensing by large-scale structures. It appears, how-

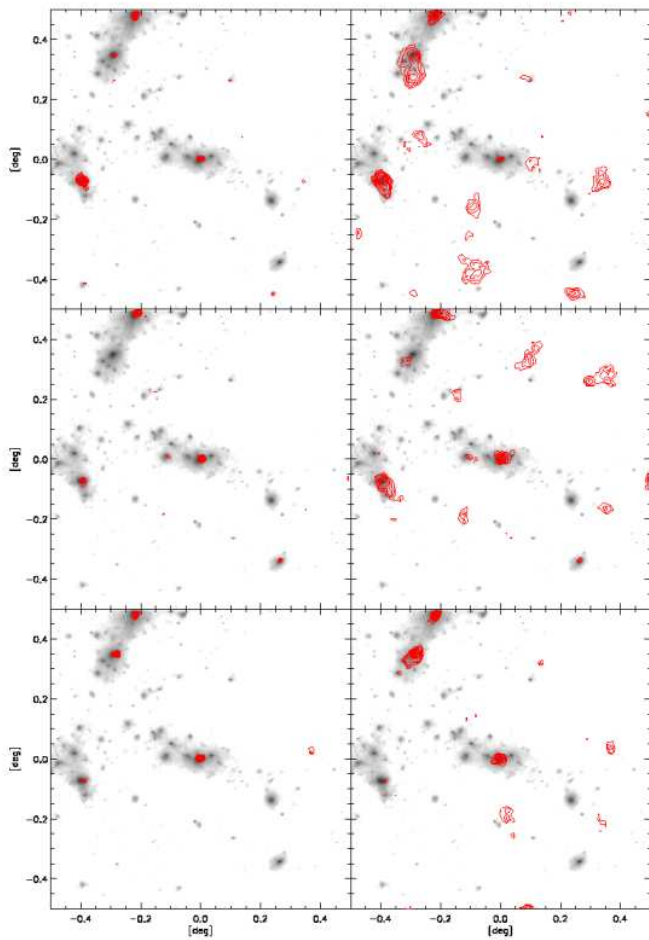


Fig. 6. As Fig. 5, but with the sources placed at redshift $z_s = 1$.

ever, from our numerical simulations that a fair fraction of the peaks found with the aperture mass may in reality not be caused by halos, but by peaks in the projected large-scale structure.

Acknowledgements. We are grateful to Catherine Heymans and Michael Schirmer for helpful discussions. The N -body simulations were performed at the “Centro Interuniversitario del Nord-Est per il Calcolo Elettronico” (CINECA, Bologna), with CPU time assigned under an INAF-CINECA grant.

References

- Bartelmann, M. 1996, *A&A*, 313, 697
 Bartelmann, M. & Schneider, P. 2001, *Physics Reports*, 340, 291
 Erben, T., Miralles, J. M., Clowe, D., et al. 2003, *A&A*, 410, 45
 Erben, T., van Waerbeke, L., Mellier, Y., et al. 2000, *A&A*, 355, 23
 Haehnelt, M. G. & Tegmark, M. 1996, *MNRAS*, 279, 545
 Hennawi, J. F. & Spergel, D. N. 2004, *ArXiv Astrophysics e-prints*
 Herranz, D., Sanz, J. L., Barreiro, R. B., & Martínez-González, E. 2002a, *ApJ*, 580, 610
 Herranz, D., Sanz, J. L., Hobson, M. P., et al. 2002b, *MNRAS*, 336, 1057
 Hockney, R. & Eastwood, J. 1988, *Computer simulation using particles* (Bristol: Hilger, 1988)
 Jenkins, A., Frenk, C., White, S., et al. 2001, *MNRAS*, 321, 372

- Maturi, M., Bartelmann, M., Meneghetti, M., & Moscardini, L. 2004, *A&A* accepted; preprint astro-ph/0408064
 Meneghetti, M., Bartelmann, M., Dolag, K., et al. 2004, *A&A*, submitted; preprint astro-ph/0405070
 Meneghetti, M., Bartelmann, M., & Moscardini, L. 2003, *MNRAS*, 340, 105
 Meneghetti, M., Bolzonella, M., Bartelmann, M., Moscardini, L., & Tormen, G. 2000, *MNRAS*, 314, 338
 Meneghetti, M., Yoshida, N., Bartelmann, M., et al. 2001, *MNRAS*, 325, 435
 Miralles, J.-M., Erben, T., Hämmerle, H., et al. 2002, *A&A*, 388, 68
 Navarro, J., Frenk, C., & White, S. 1997, *ApJ*, 490, 493
 Sanz, J. L., Herranz, D., & Martínez-González, E. 2001, *ApJ*, 552, 484
 Schaefer, B. M., Pfrommer, C., Hell, R., & Bartelmann, M. 2004, *ArXiv Astrophysics e-prints*
 Schirmer, M., Erben, T., Schneider, P., Wolf, C., & Meisenheimer, K. 2004, *A&A*, 420, 75
 Schneider, P. 1996, *MNRAS*, 283, 837
 Schneider, P., van Waerbeke, L., Jain, B., & Kruse, G. 1998, *MNRAS*, 296, 873
 Seljak, U. & Zaldarriaga, M. 2000, *ApJ*, 538, 57
 Springel, V., Yoshida, N., & White, S. 2001, *New Astronomy*, 6, 79
 Tegmark, M. & de Oliveira-Costa, A. 1998, *ApJ*, 500, L83+
 Tormen, G., Bouchet, F., & White, S. 1997, *MNRAS*, 286, 865
 Umetsu, K. & Futamase, T. 2000, in *Constructing the Universe with Clusters of Galaxies*
 Yoshida, N., Sheth, R., & Diaferio, A. 2001, *MNRAS*, 328, 669